



Title	A numerical study on the ability to predict the heat release rate using CH* chemiluminescence in non-sooting counterflow diffusion flames
Author(s)	Hossain, Akter; Nakamura, Yuji
Citation	Combustion and flame, 161(1), 162-172 https://doi.org/10.1016/j.combustflame.2013.08.021
Issue Date	2014-01
Doc URL	http://hdl.handle.net/2115/54632
Type	article (author version)
File Information	Aug_26_2013_revised_final_print.pdf



[Instructions for use](#)

**A numerical study on the ability to predict the heat release rate using
CH* chemiluminescence in non-sooting counterflow diffusion flames**

Akter Hossain and Yuji Nakamura*

Hokkaido University, Division of Mechanical and Space Engineering

N13, W8, Kita-ku, Sapporo 060-8628, Japan

*Corresponding Author:

Yuji NAKAMURA, Prof. Dr.

Division of Mechanical and Space Engineering, Graduate School of
Engineering, Hokkaido University

N 13 W 8, Kita-ku, Sapporo 060-8628 JAPAN

Tel. & Fax. +81-11-706-6386

E-mail: yuji-mg@eng.hokudai.ac.jp

Abstract:

Numerical studies on 1-D, non-sooting counterflow diffusion flames were performed to determine the precision with which the total heat release rate can be calculated using light emission, namely, chemiluminescence, from the reaction zone. A detailed reaction mechanism, incorporating sub-reaction models for excited state radicals (CH^* and OH^* , where $*$ denotes the excited state), was employed in this study. A set of 1-D, steady state conservation equations was solved under standard atmospheric conditions over a counterflow configuration utilizing the CHEMKIN-PRO package. A variety of fuels (CH_4 and C_3H_8), velocities (0.1 m/s – near the extinction condition), diluents (N_2 , H_2O , CO_2 , and Ar), detailed reaction mechanisms for C_1 - C_3 hydrocarbons (GRI-Mech 3.0, Hai Wang's-, and San Diego-mechanism), different sub-reaction models for excited radicals, and excited radical transport properties were examined for the current purpose. It was found that a one-to-one correlation between total chemiluminescence from CH^* and the total heat release rate cannot be sustained when the flame experiences a relatively high stretch and dilution, even though the condition is still far away from extinction. This trend is consistent with the different types of fuels, and it is understood that the reduction of the ethynyl radical (C_2H), a potential precursor of CH^* , is the main cause of the one-to-one correlation not being sustained. To this end, it was concluded that the observable light emission can only be used to predict the total heat release rate when non-sooting diffusion flames exist under velocity conditions from 0.1 m/s to 1.5 m/s. In other words, the chemiluminescence intensity does not always correlate with the total heat release rate of highly stretched flames found in practical combustors.

Keywords: chemiluminescence, excited state radical (CH^*), diffusion flame, flame diagnostics

1. Introduction

1.1 Heat release rate: How can it be indirectly predicted?

Most of the unsteady combustion found in practical combustors takes place under a highly turbulent flow environment, making diagnosis of the instantaneous combustion status a difficult task. The heat release rate is considered an important quantity to characterize the strong reactive region and to also predict and control unsteady combustion behaviors [1-6]. Direct measurement of the heat release rate is not easy [7] because currently available measurement techniques are not sophisticated enough to be applied in practical combustors. Because of this, the natural emitted light, i.e. chemiluminescence from chemically excited radicals such as CO_2^* , C_2^* , CH^* and OH^* (where * denotes the excited state), has traditionally been used to predict the heat release rate of flames [8-23]. Since the measurement of chemiluminescence is relatively simple and non-intrusive compared to other diagnostic tools, many researchers have paid attention to chemiluminescence, not only to study the fundamentals of flame science but also to monitor the combustion status in practical uses. Numerous numerical and experimental studies on chemiluminescence-based prediction of the heat release rate of flames have been performed throughout the decades and are briefly reviewed and classified below.

1.2 Brief review of past studies

1.2.1 Predicting the heat release rate via CO_2^* and C_2^* chemiluminescence

The most extensive numerical study on chemiluminescence emission from CO_2^* in methane- and propane-air premixed flames was performed by Samaniego et al. [9] over a wide range of conditions. They found a quantitative correlation between the *integrated* chemiluminescence emitted from CO_2^* and *integrated* heat release rate. Later, in an experimental study, Samaniego et al. [10] successfully predicted the *integrated* heat release rate over the entire domain using the CO_2^* emitted *integrated*

chemiluminescence in the vortex-induced, strongly perturbed, methane- and propane-air premixed turbulent flames. Hardalupas et al. [11] found in their experimental study of a natural gas-air premixed flame that the local chemiluminescence intensity from CO_2^* could be considered a good indicator of the local heat release rate, whereas C_2^* was not a dependable indicator. A numerical study by Kathrotia et al. [12] on a methane-air premixed flame also concluded that C_2^* was not a dependable indicator. The excited radical, CO_2^* , was instead found to be the main chemiluminescence emitter in lean flames, whereas C_2^* was the dominating emitter in rich flames. Therefore, in between these two extreme fuel conditions, chemiluminescence emitted from both CO_2^* - and C_2^* -radicals might not be suitable for prediction of the heat release rate of flames under a wide range of conditions. In other words, they would not be the best candidates to predict the heat release rate of non-premixed flames, where the local mixture condition is not prescribed or known.

1.2.2 Attempts to predict heat release rate via OH^* and CH^* chemiluminescence

Hardalupas et al. [11] and Kathrotia et al. [12] both reported that the local chemiluminescence intensity from OH^* and CH^* radicals was an important indicator of local heat release rate. A recent experimental study by Hardalupas et al. [13] on DME and methane Bunsen flames concluded that the local chemiluminescence from OH^* and CH^* can successfully identify the local heat release rate. Haber et al. [14] experimentally examined the Bunsen- and honeycomb-burner flames of methane and reported that OH^* was a good indicator of the local heat release rate, whereas CH^* was not adequate, contradicting the findings of Hardalupas et al. [11, 13] and Kathrotia et al. [12]. Nori and Seitzman [15] reported that although the *integrated* chemiluminescence from CH^* scaled with the local heat release rate in lean premixed hydrocarbon flames, it depended on the local equivalence ratio and pressure. Lauer et al. [16] concluded that the integral of the heat release rate correlated with the integral of the

chemiluminescence intensities because of either OH* or CH* in the turbulent premixed methane-air flames. In addition, they reported that neither OH* nor CH* were reliable measures of the local heat release rate distribution in flames. Farhat et al. [17] experimentally examined propane diffusion (non-premixed) jet flames, which were disturbed by standing waves. They suggested that OH* and CH* might not be reliable indicators of the local unsteady heat release rate in flames. Ayoola et al. [18] reported in an experimental study of ethylene-air turbulent premixed flames that chemiluminescence emitted from OH* was not a reliable indicator of the local heat release rate. A recent study by Lauer et al. [19] concluded that the local chemiluminescence from OH* in turbulent methane-air premixed flames correlated with the local heat release rate. The most recent experimental studies by Röder et al. [20, 21] found that the local heat release rate correlated with the spatially *integrated* OH* emitted chemiluminescence in turbulent methane-air premixed flames. Papoutsos et al. [22] observed in their numerical study that the local chemiluminescence due to the excited radicals (CH* and OH*) could to be used as a marker of the local heat release rate for non-premixed flames in severely stretched conditions. On the contrary, the numerical results of Najm et al. [23] in premixed flames revealed that the local chemiluminescence from excited radicals (CH* and OH*) was generally not a reliable indicator of the local heat release rate in a highly curved flame zone.

As summarized, the results obviously contradict each other; in fact, the studies of Hardalupas et al. [11, 13] and Ballester [24] clearly emphasize the need for further investigation to clarify the contradictory conclusions.

1.3 What should be investigated further? Motivation of the present work

It is well known that excited radicals, such as CH^* and OH^* , emit light from the combustion zone at visible and ultraviolet wavelengths, respectively. Measurement of the visible light emission from CH^* requires conventional optical systems. However, to measure ultraviolet light from OH^* an intensified IR CCD camera and specially designed optical system are essential. Because of this advantage, the chemiluminescence from CH^* should be the most convenient and efficient way to diagnose the heat release status in practical combustors. This is one motivation to focus on CH^* in this study.

From the survey of past work, found in section 1.2, it is obvious that the variety of contradictory arguments and conclusions were drawn under a variety of conditions such as limited types of fuel, strain rates, diluents. Moreover, the majority of the above studies were performed considering premixed or partially premixed flames, and studies on the diffusion flames were rarely performed [17]. The reason for limited studies on diffusion flames may be because of soot production in typical hydrocarbon-air diffusion flames. The continuous spectrum emissions (i.e., thermal radiation) from the soot can mask the light emitted from excited radicals. However, if one can separate the emission from the soot and chemiluminescence via an optical method or if the target flame is a non-sooting diffusion flame (namely, hydrogen-mixed fuel flames, oxygenated fuel flames, highly diluted fuel flames, pre-heating supported mild flames, and micro-scale flames with a flame height less than the smoke point), finding a correlation between the chemiluminescence and heat release in the system would be quite valuable. For instance, optical access to micro-scale diffusion [26] and highly turbulent diffusion flames [27] to estimate their combustion performance is quite difficult, especially at near extinction

conditions. Because of this, chemiluminescence-based diagnostics have the potential to play a vital role in the study of limiting non-premixed flames.

Additionally, the literature review revealed that various treatments are used to determine thermodynamic and transport properties for excited radicals since those properties are not well understood and not readily used. For example, Hirschfelder et al. [28] reported that the collision diameters of excited species were significantly larger than the same species in their ground state. Therefore, potential-well depths for those excited radicals were expected to vary accordingly. However, Leo et al. [25], Kojima et al. [29], and Hall et al. [30] assumed no difference between the ground- and excited-state radicals in terms of their thermodynamic and transport properties. Therefore, because of the lack of unified evidence and data currently in the open literature, an arbitrary variation in the transport properties of the excited radicals was made to further examine their influence on the target results in this study.

1.4 Objectives of the present study

The aim of the present study is to numerically investigate the total chemiluminescence capability of CH^* to predict total heat release rates in 1-D, non-sooting, counterflow diffusion flames. Methane (CH_4) and propane (C_3H_8) were chosen as fuels for the study since their combustion chemistries are well established, and they are widely used in practical combustion systems. The influence of a variety of relevant numerical parameters such as applied reaction mechanisms for ground and excited state species, applied velocity, diluents, and the transport properties of excited radicals, on the relationship between total heat release rate and total chemiluminescence from CH^* was explored. Using the present investigations, the ability to predict the heat release status in practical combustors by chemiluminescence is discussed.

2. Numerical Method

2.1 Applied numerical model

In this work, steady state, 1-D, non-sooting counterflow diffusion flames were studied under standard atmospheric conditions. The distance between the burners (L) was set to 2.0 cm, and the initial temperature for fuel and oxidizer flow was kept at 300 K. The widely used hydrocarbon fuels, methane (CH_4) and propane (C_3H_8), were supplied from the fuel port, while dried air (a mixture of N_2 and O_2) was supplied from the oxidizer port. The fuel was diluted by the inert gas species, such as nitrogen (N_2), water vapor (H_2O), carbon dioxide (CO_2), or argon (Ar), to examine their influence on the predicted results. The governing steady state 1-D transport equations were solved numerically by the CHEMKIN-PRO package [31] using detailed chemical reaction models for ground state species and incorporating the various sub-reaction mechanisms for excited state species (CH^* and OH^*), which are described in the following section. Applied flow velocity (V), which is used to modify the stretch rate of flames, is considered an important numerical parameter. The considered range was near the extinction limit (e.g. 0.1 m/s – 3.0 m/s for methane-air flames). The velocity ratio was set to unity so that the stretch rate, k , could be defined as $k = 2V / L$.

2.2 Chemical reaction mechanisms for ground- and excited-state species

To ensure a general correlation between the total observable chemiluminescence and total heat release rate, several reaction models were considered in this study. The detail chemical reaction mechanisms, for the production/consumption of ground state species, employed were GRI-Mech 3.0 [32], Hai-Wang-Mech (HW-Mech) [33], and San Diego Mech (SD-Mech) [34]. In addition, two excited radicals, such as CH^* and OH^* , (where $*$ denotes the excited state) were included in this numerical study. Accordingly, to clarify their effects, several sub-reaction models for excited species (CH^* and OH^*) proposed by Panoutsos et al. [22], Kojima et al. [29], Nori et al. [35], and Walsh et al.

[37] were also considered. For example, the sub-reaction model and its associated reaction rate parameters proposed by Nori et al. [35] for the production/consumption of the excited radicals are listed in Table 1. The reactions listed in Table 1 along with the species C_2H , OH^* , and CH^* are added to the detailed kinetics model (e.g. GRI-Mech 3.0). Throughout this study, the combination of GRI-Mech 3.0 [32] and Nori's sub-reaction model [35] is considered as "basic" and used unless otherwise specified.

Thermodynamic properties for the excited radicals, namely CH^* and OH^* , were taken from Burcat's thermodynamic data [38]. The transport properties for CH^* and OH^* were considered to be the same as their ground state, CH and OH , throughout the study unless otherwise described. Note that this assumption does not have any concrete theory available to support it. To examine the validity of this assumption in the present study, the Lennard-Jones collision diameter, σ , and Lennard-Jones potential well depth, ε , were arbitrarily varied to examine their sensitivity to the predicted results. The combinations of different potential parameters, σ and ε , considered in this study are summarized in Table 2.

2.3 Numerical computation of chemiluminescence from excited radicals

According to Nori et al. [15, 35, 36], the photon emission rate (mole photons/($cm^3 \cdot s$)) from an excited species (CH^*) is estimated using the following equation:

$$I_{CH^*} = A \times [CH^*] \quad (1)$$

where $[CH^*]$ is the concentration of CH^* and A is the Einstein coefficient ($A = 1.85 \times 10^6 \text{ s}^{-1}$ [39]) for spontaneous emission during the transition of CH^* back to its ground state, i.e. CH^* (excited state) \rightarrow CH (ground state). The numeric value of the Einstein coefficient has been validated in refs. 15, 35, and 36 and was found to be satisfactory. To produce chemiluminescence emissions from CH^* as per unit flame area

(mole photons/(cm²·s)), the computed CH*-photon emission profile across the flame was integrated over the entire numerical domain, L , and the integral is given by following equation:

$$TCL = \int_0^L I_{CH^*} dx \quad (2)$$

where L is the burner distance (entire numerical domain) and TCL (mole photons/(cm²·s)) stands for total chemiluminescence emitted from the flame.

3. Results and discussion

3.1 Flame structure under different sub-reaction models for excited radicals

Figure 1 shows the typical flame structure, without dilution, of the diffusion flames for various types of fuels (CH₄ and C₃H₈) subjected to different sub-reaction models for excited radicals. Only the case with an ejection velocity of 0.5 m/s is shown as a representative figure. It is obvious from this figure that the concentration profile of CH* matches the profile for the heat release rate over a narrow zone, irrespective of the type of fuel. Moreover, it is clear that the sub-reaction models for excited radicals do not exhibit any significant influence on the profiles of the fuel, oxidizer, heat release, and temperature. However, the sub-reaction models are sensitive to the concentration profiles of CH* over the flame structures for hydrocarbon fuels. Upon further inspection, it was found that the sub-reaction models proposed by Walsh et al. (1998) and Kojima et al. (2005) produce almost identical profiles for the CH*-concentration, and the sub-reaction models proposed by Nori et al. (2008) and Panoutsos et al. (2009) produce identical profiles for CH*. The significant deviation in the predicted CH*-concentration by these two groups (Walsh-Kojima and Nori-Panoutsos) could be because of different reaction paths to modify the production/consumption rate of CH* in each group.

The concentration of CH* shows a single, sharp, positive peak, which coincides with the positive peak of the heat release rate. As expected, the zone with the heat

release is relatively narrow and concentrated in the so-called reaction zone. Accordingly, most of the consumption of CH* is also concentrated around this region in the hydrocarbon flames.

Figure 2 shows the profiles of the major production/consumption rates of CH* in typical methane- and propane-air flames. In Fig. 2, the same numerical conditions (no dilution, ejection velocity of 0.5 m/s, and different sub-reaction models for excited radicals) used for Fig. 1 are applied. It is understood in Fig. 2 that CH* is generated through the oxidation reaction of an ethynyl radical (C₂H) with an O atom and O₂ molecule, respectively ($C_2H + O \rightarrow CH^* + CO$; $C_2H + O_2 \rightarrow CH^* + CO_2$), while a major amount of it is mainly consumed by collision with N₂ ($CH^* + N_2 \rightarrow CH + N_2$). Moreover, it was observed that the oxidation reaction, $C_2H + O \rightarrow CH^* + CO$, played a major role in producing CH*, while the reaction, $C_2H + O_2 \rightarrow CH^* + CO_2$, played a negligible role in the production of CH* for the sub-reaction models proposed by Walsh et al. (1998) and Kojima et al. (2005). On the contrary, the reaction $C_2H + O_2 \rightarrow CH^* + CO_2$ played a slightly higher role in producing CH* compared to the $C_2H + O \rightarrow CH^* + CO$ reaction for the sub-reaction models proposed by Nori et al. (2008) and Panoutsos et al. (2009). These trends are consistent irrespective of fuel type. In addition, a clear deviation is seen in the peak value and peak position for the major production/consumption rate of CH* for different sub-reaction models and fuels. This feature is consistent with the concentration profile trend of CH* shown in Fig. 1. Although not shown here, the same trend was found when fuel dilution by 50% and 70% of nitrogen (N₂) was employed, suggesting that the collision partner (N₂) for major CH*-consumption is produced by the nitrogen on the oxidizer side.

Figure 3 represents the influence of detail reaction mechanisms on the major production/consumption rates of CH* over a wide range of velocities for a non-diluted methane-air flame. It was observed for all detail reaction mechanisms, that the

production of CH* increases with increasing applied velocity up to the moderate velocity regime. Consequently, the consumption of CH* follows the same trend as the production of CH* in the moderate velocity regime. In the high velocity regime, production/consumption decreases because of low levels of C₂H production (This will be clarified later.), as the excited radical, CH*, is mainly produced through the following reactions: C₂H + O → CH* + CO and C₂H + O₂ → CH* + CO₂. Furthermore, it was found that the overall production/consumption rates of CH* by HW-Mech [33] and GRI-Mech 3.0 [32] were very close to each other, while for SD-Mech [34] was comparatively low because of the insufficient production of CH* precursors.

3.2 Correlation between local heat release rate and local concentration of CH*

To look for a correlation between the heat release rate and potential chemiluminescence intensity the local versus local relationship was first investigated. Figure 4a shows the correlation between the local concentration of CH* and local heat release rate in the non-diluted methane-air flame for various velocity conditions. It should be mentioned that this local concentration of CH* was utilized to estimate the chemiluminescence intensity. This figure clearly shows that the increment of the CH* concentration also leads to an increase in the local heat release, and the gradients of these profiles changed with the increment of the applied velocity. More importantly, the local heat release was expressed as a multi-valued function of the local concentration of CH*. The appearance of the looping/multi-valued behavior in the [CH*]-HRR phase plane was caused by the existence of different characteristics between the two profiles, for example, the heat release rate (HRR) and concentration of CH* ([CH*]) for a certain applied velocity, either 0.5 m/s or 1.0 m/s, at a certain location over the distance from the fuel port, as shown in Fig. 4b. This type of looping characteristic, seen in Fig. 4a, was also found by Gazi et al. [7] in their study on the ability of chemical markers to

assess heat release rates in laminar premixed flames. However, the looping characteristics cannot be used for a one-to-one correlation between chemical markers and heat release rate, which was desirable for practical purposes.

Therefore, based on the target in this present study, the looping/multi-valued characteristics suggest that solely tracking CH* cannot predict the local heat release rate. A local CH* measurement is not a reliable tool to diagnose the local heat release status. Of course, the next choice would be utilization of total chemiluminescence from CH* to predict the local heat release rate. This is because chemiluminescence is recognized as a promising, observable quantity, but the heat release rate is not, making direct measurement difficult [7]. The *total chemiluminescence* versus *local heat release rate* correlation depends on the spatial information. Therefore, employing this method in practical combustors where combustion usually occurs under high turbulent conditions is not possible. As a result, in particular from a practical application point of view, total chemiluminescence information would be a more convenient and realistic method to diagnose the total heat release rate status in practical combustors system. Therefore, in the following section, based on Lauer et al. [16], the applicability of total chemiluminescence, emitted by CH*, to predict the total heat release rate of flames is examined.

3.3 Correlation between integrated chemiluminescence from CH* (total chemiluminescence) and integrated heat release rate (total heat release rate)

3.3.1 Influence of fuel types

Figure 5 shows the correlation between total chemiluminescence and the total heat release rate when subjected to various fuels and a wide range of velocity conditions. In

both methane (CH_4) and propane (C_3H_8) fuels, the total heat release rate increased linearly as the total chemiluminescence increased within the moderate velocity range. A further increase in the imposed velocity resulted in the correlation slightly “bending” toward the left in the figure, namely, towards smaller total chemiluminescence values. The gradient of the linear relationship was influenced by the fuel type. This suggested that the chemiluminescence intensity is highly sensitive to the fuels burned.

3.3.2 Influence of the detail chemical mechanisms for ground state species

Figure 6 shows the influence of a detail reaction mechanism on the correlation between total chemiluminescence from CH^* and the total heat release rate over a wide range of applied velocities as depicted in Fig. 5. From the figure, it is understood that the overall trend, a linear relationship followed by a “bending” feature as stated previously, is generally irrespective of the applied reaction models. In addition, it can be seen that the prediction of the target correlation by HW-Mech [33] is very close to the one by GRI-Mech 3.0 [32] irrespective of the fuel type considered in this study. However, the one by SD-Mech [34] exhibits a significant deviation. This issue will be further addressed later. Next, the influence of pertinent parameters on the correlation was investigated. For the present purpose, only a methane-fuel was considered.

3.3.3 Influence of sub-reaction models for excited radicals

Figure 7 shows the influence of the sub-reaction models for excited radicals on the correlation between total chemiluminescence from CH^* and total heat release rate. As a representative example, the cases for non-diluted methane fuel were considered under a wide range of velocities. Again, it was confirmed that the sub-reaction model does not exhibit any significant influence on the overall correlation trend; namely, the linear relationship holds in the moderate velocity regime and a non-linear relationship appears in the higher velocity regime. However, the correlation gradients depend on the sub-

reaction models which are supposed to be caused by different levels of production/consumption of CH^* via different reactions paths, as shown in Fig. 2.

3.3.4 Influence of diluents

Figure 8 shows the influence of various diluents on the correlation between the total chemiluminescence from CH^* and total heat release rate for methane fuel over a wide range of velocities. It was seen that a linear relationship exists between the total chemiluminescence and total heat release rate within the moderate velocity regime, for all dilution conditions except those highly diluted by N_2 . At higher velocities, the linear curve tends to bend toward the lower values of chemiluminescence. Although the critical velocity resulting in the bending correlation curve varies according to the dilution, the overall trend of the relationship remains unchanged. In fact, this is consistent with different types of diluents (N_2 , H_2O , CO_2 , and Ar), showing that the type of diluent does not govern the trend, i.e. up to a certain critical velocity the relationship is linear, and at higher velocities the relationship is non-linear. Of course, because diluents were added to fuel, the local flame chemistries, including the production/consumption chemistries of the excited radical and its precursor chemistries, were changed. Consequently, the maximum flame temperature, near extinction condition of the flame, heat release rate, concentration of precursor (C_2H) for the excited radical (CH^*), and concentration of CH^* were significantly reduced. Therefore, drastic changes, regarding the total heat release rate and total chemiluminescence values, in the target correlation were observed when a higher percentage of diluent was added to the fuel. However, even under such drastically changed conditions, the overall tendency of the correlation was conserved. Additionally, the gradient of the relationship was slightly influenced by the diluents, the bending feature was pronounced in diluted fuel, and deviation from the linear line (non-dilution case) depends on the diluents. Therefore, it was suspected that the observed “bending” feature might be related to the

extinction. It is worthy to note that the bending of the linear relationship in the high velocity case is somehow similar to what was reported by Najm et al. [23]; although, their target was a premixed flame and the breaking source was not the stretch but the curvature or something else.

3.3.5 Influence of transport properties

The transport properties, mainly the Lennard-Jones collision diameter, σ , & Lennard-Jones potential well depth, ε , for ground state CH and OH are used for their excited states, CH* and OH*, respectively. This is termed as *Case I* while other combinations are referred to as *Case II – Case V*, and all of these detailed combinations are listed in Table 2. Figure 9 shows the influence of σ and ε on the target correlation without a dilution effect under velocity conditions ranging from 0.1 m/sec – 3.0 m/sec and subjected to various combinations for σ and ε ranging from *Case I – Case V*. It is clear from the figure that the variations of the Lennard-Jones collision diameter, σ , (i.e. *Case II and Case III*) and Lennard-Jones potential well depth, ε , (i.e. *Case IV and Case V*) on the target correlation exhibit exactly the same behavior as *Case I*, which reveals that the transport properties, σ and ε , are insensitive to chemiluminescence emission characteristics and the heat release rate in diffusion flames. Therefore, in the following sections, the transport properties listed for *Case I* in Table 2 will be used unless it is otherwise specified.

3.4 Deviation and bending feature in total chemiluminescence versus total heat release rate correlation

3.4.1 Cause of deviations among the predictions (*total chemiluminescence versus total heat release rate correlation*) by the detailed reaction mechanisms (GRI-Mech 3.0 [32], HW-Mech [33], and SD-Mech [34])

As observed in Fig. 6, there is a significant deviation in the total chemiluminescence versus total heat release rate correlation prediction by SD-Mech [34] compared to GRI-Mech 3.0 [32] and HW-Mech [33]. To determine the cause of the deviation, the common trend of the decomposition reaction paths producing the excited radical, CH*, from different fuels, irrespective of the applied reaction models, must be identified. Then the behavior of the precursor, ethynyl radical (C₂H), must be examined since it was found to be the vital species for production of CH* in all sub-reaction models applied in this study (see Table 1).

Figure 10 shows the major reaction paths by which the excited radical, CH*, is produced from the methane-air and propane-air flames. It is understood for both methane- and propane-air flames that acetylene (C₂H₂) is the main trigger to produce the ethynyl radical (C₂H) which is the precursor of the excited radical, CH*. The same reaction paths and triggers for the ethynyl radical (C₂H) seen in Fig.10 are also confirmed when using the SD-Mech [34] and HW-Mech [33] methods (Data not shown). This observation proves that the following sequence: “fuel → =.... → C₂H₂ → C₂H → CH*,” is a common reaction pathway to produce CH*, irrespective of the fuel type or applied reaction model. Additionally, once the ethynyl radical (C₂H) is produced in the system, the oxidation reactions, C₂H + O → CH* + CO and C₂H + O₂ → CH* + CO₂, occur and produce CH*, which directly determines the intensity of light emission as chemiluminescence.

Figure 11 shows the production of the precursor ethynyl radical (C₂H) in the methane-air flames when three different detail reaction mechanisms (GRI-Mech 3.0 [32], HW-Mech [33], and SD-Mech [34]) are applied at a velocity of 0.5 m/s. It is understood that the prediction of C₂H production by HW-Mech [33] is close to GRI-Mech [32], but the prediction by SD-Mech [34] has only half the peak value obtained by applying GRI-Mech [32]. Although it is not shown here for brevity, identical profiles

for the ethynyl radical (C_2H) are observed in the case of propane-air flames when the above detail reaction mechanisms are employed. The results presented in Fig. 11 are match well with the deviation observed in the correlation between total chemiluminescence and total heat release rate depicted in Fig. 6. Thus, it can be concluded that the deviation (in Fig. 6) is directly caused by insufficient production of the precursor, ethynyl radical (C_2H) through the reactions involved in SD-Mech [34].

In the next section, the cause of the ‘bending feature’ observed in the correlation between total chemiluminescence and total heat release rate presented earlier for a wide range of conditions will be examined. However, before exploring the cause of the bending feature, it is important to note one of the important features of the pure methane-air flames is that they do not easily generate soot [40] compared to other hydrocarbon fuels when polycyclic aromatic hydrocarbons (PAHs) are formed. It is possible that the addition of PAH formation kinetics in the pure methane-air flame may affect the concentration of C_2H_2 (as C_2H_2 is consumed to produce PAHs) and thus the concentration of C_2H , which is a precursor for CH^* formation (see Fig. 10). Therefore, whether the target correlation for the total chemiluminescence and total heat release rate still holds when polycyclic aromatic hydrocarbons (PAHs) formation kinetics are taken into account must be determined. To clarify this issue, the behavior of chemiluminescence emissions from CH^* in pure methane-air flames subjected to the addition of PAHs kinetics, proposed by Wang et al. [41], was examined. The peak values for the mole fraction of CH^* with and without PAH addition for pure methane-air flames were compared and are shown in Table 3. The comparison shows that the difference between the mole fraction of CH^* in both cases is less than 10% at different applied velocities. It is also clear from Table 3 that the peak value of the mole fraction of CH^* increases as the applied velocity increases in both cases, and the maximum mole fraction peak value is attained at a velocity of 2.0 m/s. If the velocity is then further

increased the mole fraction of CH^* decreases. These results indicate that the total chemiluminescence emissions due to CH^* will not be reduced more than 10% when PAHs are added, and the target correlation between total chemiluminescence and total heat release rate will hold even if PAH formation is added to pure-methane air flames.

3.4.2 Cause of the “bending” feature in the correlation between total chemiluminescence and total heat release rate

It was found in the preceding sections (e.g. Figs. 5-9), that the linear relationship between the total chemiluminescence intensity and total heat release rate holds over moderate velocities (i.e. stretch rate). However, as the velocity increases (i.e. the stretch rate becomes stronger) a “bending” feature appears. The cause of this important feature is discussed in the following section.

It should be noted that the common response of a flame subjected to high stretch and dilution is a reduction in flame temperature. The applied velocity response on maximum temperature (T_{max}), total chemiluminescence (TCL), and total heat release rate (THRR) with/without dilution effect is presented in Fig. 12. Fig. 12 shows that as the applied velocity increases the maximum temperature decreases. Importantly, the total chemiluminescence follows the trend for the total heat release rate in the lower velocity regime but not in the higher velocity regime. Instead, it follows the behavior of the maximum temperature. Thus, it is suspected that the “bending” feature could be closely related to the production/consumption of CH^* .

It is also true that increases in the applied velocity not only reduce flame temperature; they also affect flame chemistry, including the production/consumption rate of CH^* . As noticed in Fig. 10, acetylene (C_2H_2) is the dominant molecule to produce the ethynyl radical (C_2H), a precursor for production of CH^* . Indeed, the earlier studies by Mével et al. [42] revealed that the behavior of excited radicals is very sensitive to the behavior of any precursor-species. This evidence indicates that a

molecule that influences the behavior of the precursor-species could play a significant role in changing the characteristics of the excited species. Hence, in the following section, three topics are examined, first, the sensitivity of the reaction paths which produce the precursor (C_2H) for CH^* from the triggering molecule (C_2H_2); Second, how the precursor molecule (C_2H) is consumed to generate the excited radical (CH^*), and finally, the influence of the applied velocities over a wide range, 0.1 m/s – 3.0 m/s, on the C_2H reaction paths during the event of combustion.

Figure 13 shows the sensitivity of the reaction paths for the production/consumption of C_2H for a methane-air flame without a diluent at an applied velocity of 0.5 m/s. It is apparent in Fig. 13 that the reaction, $OH + C_2H_2 \rightarrow C_2H + H_2O$, is the main reaction of the reactions that produce the precursor, C_2H . There are other reaction paths, such as, $O + C_2H_2 \rightarrow OH + C_2H$ and $C + C_2H_2 \rightarrow C_2H + H$, which also contribute to the production of C_2H , but their contributions are minor compared to the first reaction. It was estimated that the aggregated contribution of the two reactions, $O + C_2H_2 \rightarrow OH + C_2H$ and $C + C_2H_2 \rightarrow C_2H + H$, in producing C_2H is still seven times lower than the contribution from the reaction, $OH + C_2H_2 \rightarrow C_2H + H_2O$. It is clear that the precursor, C_2H , is consumed via different reactions but only the reactions $C_2H + O_2 \rightarrow CH^* + CO_2$ and $C_2H + O \rightarrow CH^* + CO$ produce the excited radical CH^* by consuming C_2H during the combustion process. Besides, the consumption of C_2H proceeds through other reactions, such as, $C_2H + O_2 \rightarrow HCO + CO$, $OH + C_2H \rightarrow H + HCCO$, and $O + C_2H \rightarrow CH + CO$, is much higher compared to the consumption of C_2H via the reactions $C_2H + O_2 \rightarrow CH^* + CO_2$ and $C_2H + O \rightarrow CH^* + CO$. However, the higher consumption of C_2H by the previously mentioned reactions does not produce the excited radical (CH^*), and the transition of the excited radical (CH^*) to its ground state is used to predict heat release via emission of visible light. Hence, in the next section, the influence of the applied

velocities on the production of C₂H and consumption of C₂H in producing CH* are examined.

Figure 14 represents the peak production/consumption behavior of C₂H and the peak values for the mole fraction of CH* over a wide range of applied velocities for a methane-air flame without diluent. It should be noted here that the peak values for the mole fraction of CH* were collected from the profiles of the mole fraction distribution against applied velocities, which is shown in the next section (see Fig. 15). Each peak value of CH* for the corresponding applied velocities is then superimposed into Fig. 14 to understand the close correlation between the consumption of precursor (C₂H) and production of CH* (due to the consumption of C₂H) over the wide range of applied velocities. At first, the velocity response to the total production of C₂H via reactions, which are R - #A ($\text{OH} + \text{C}_2\text{H}_2 \rightarrow \text{C}_2\text{H} + \text{H}_2\text{O}$), #B ($\text{O} + \text{C}_2\text{H}_2 \rightarrow \text{OH} + \text{C}_2\text{H}$), and #C ($\text{C} + \text{C}_2\text{H}_2 \rightarrow \text{C}_2\text{H} + \text{H}$), was examined. It is clear that the peak values for the total production of C₂H increase as the applied velocity increases up to 2.0 m/s. Above 2.0 m/s the values decrease with increasing velocity. Next, the consumption of C₂H to produce CH* via $\text{C}_2\text{H} + \text{O}_2 \rightarrow \text{CH}^* + \text{CO}_2$ and $\text{C}_2\text{H} + \text{O} \rightarrow \text{CH}^* + \text{CO}$ was examined. It can be clearly seen that the behavior of the C₂H consumption against the applied velocity is the same observed in the total production of C₂H by reactions, such as, #A, #B, and #C. At last, the behavior of the mole fraction of the excited radical (CH*) is seen to follow the trend of the consumption/production of C₂H against the applied velocities via different reactions paths as mentioned above. As summarized, the overall behaviors of the production/consumption of the precursor molecule, C₂H, and the mole fraction of CH* over the entire applied velocity are consistent, i.e. production/consumption of C₂H and the mole fraction of CH* increase over the velocity range 0.1 m/s – 2.0 m/s and decrease in the velocity regime higher than 2.0 m/s, and all of the quantities attain their maximum at a velocity of 2.0 m/s. In the higher velocity

regime, the reduction in C_2H production directly reduces the consumption of C_2H to produce CH^* . As a result, the concentration of CH^* is reduced and light emission from CH^* in the flame is reduced. This observation matches with the correlation “bending” feature observed in Figs. 5-9 for the higher velocity regime.

Figure 15 shows the behavior profiles of CH^* over a range of distances from the fuel port against a range of applied velocities for methane-air flames. The behavior of the peak values from the mole fraction profiles of CH^* against applied velocity are superimposed in Fig. 14 and have been explained in the previous section. Additionally, it was found in Fig. 15 that the broadness of the mole fraction profile of CH^* was reduced, along with peak values, as the applied velocity was increased. Hence, in the high velocity regime, the broadness of the CH^* ($[CH^*]$) concentration profile and peak values will be reduced accordingly. The reductions in those two quantities directly contribute to the reduction in integrated chemiluminescence, i.e. the total chemiluminescence in the high velocity regime, and this is consistent with what was previously observed. Furthermore, it was observed that no value of CH^* exists (see velocity of 3.0 m/s) at the fuel side (lower than the distance of approximately 0.875 cm from the fuel port) as the precursor (C_2H) is not available in that zone (see Fig. 17), which signifies no light emission is expected as the flame goes to extinction after a velocity of 3.0 m/s.

Besides, it was noticed in Fig. 13 and Fig. 14 that the acetylene molecule (C_2H_2) reacts with the OH-molecule, O-atom, and C-atom. Those reactions produce the precursor of CH^* (C_2H), which is reduced in the high velocity regime. Therefore, the next section examines the behavior of the mole fraction of C_2H_2 against applied velocities.

Figure 16 represents the mole fraction profile for acetylene (C_2H_2) over a wide range of applied velocities for non-dilute methane-air flames. It can be clearly seen in Fig. 16 that the mole fraction of acetylene (C_2H_2) is reduced as the applied velocity increases. In addition, the broadness of the profile decreases, because of the force-like compression acting on the point around 0.875 cm, when the applied velocity increases. This observation is consistent with the experimental and numerical conclusions made by Böhm et al. [40] on PAH formation features in strained counterflow diffusion flames. This might be because the temperature decreases monotonically as the velocity increases, as seen in Fig. 12. The reduction and the sharp rise in the mole fraction profile of C_2H_2 in the higher velocity regime results in limited C_2H_2 availability in the oxidizer zone (> 0.875 cm). This limited amount of C_2H_2 reacts with OH ($C_2H_2 + OH \rightarrow C_2H + H_2O$), which is the dominating reaction to produce C_2H , see Fig. 13) as shown in Fig. 17 and produces less C_2H which eventually produces a smaller amount of CH^* . This is a reason for the sudden decrease in CH^* as the velocity increases.

Finally, Fig. 18 shows the numerical and experimental comparison, over the applied velocity conditions from 1.0 m/s to 3.5 m/s, between the peak of the mole fraction of CH^* for methane-air flames from the present study with that from the study of Prabasena et al. [43]. It is clear in Fig. 18 that the peaks do not agree [43]. However, the behavior of the peak value under the applied velocity conditions qualitatively agrees with the peak observed in the study of Prabasena et al. [43].

4. Conclusions

In this study, 1-D, non-sooting counterflow diffusion flame calculations were performed over a wide range of conditions to examine the feasibility of predicting the total heat release rate in practical combustors from the total observable light emitted by the reaction zone. From this investigation the following conclusions can be drawn:

1. The predicted total chemiluminescence emission from methane-air and propane-air diffusion flames correlates linearly with total heat release rate for velocity conditions from 0.1 m/s to 1.5 m/s; At higher velocities, >1.5 m/s, and highly diluted fuel conditions a non-linear relationship is observed.
2. The main cause of non-linearity in the high velocity regime is reduction of the precursor, i.e. the ethynyl (C_2H) radical to produce the excited state of CH (CH^*), via reduction of acetylene (C_2H_2) and the different temperature sensitivity of the total chemiluminescence and total heat release rate.

Overall, the linear correlation between the total observable light emission and total heat release rate is ensured for the velocity regime ranging from 0.1 m/s to 1.5 m/s for methane-air and propane-air diffusion flames over a wide range of conditions. Therefore, under velocity condition ranging from 0.1 m/s to 1.5 m/s, it is expected that the total observable light emission can be utilized to predict the total heat release rate in non-sooting, diffusion flames in practical combustors without the instrumental complications encountered using conventional optical measurement techniques. However, when combustion takes place under very severe conditions (with high stretch and local extinction), it is difficult to conclude that the chemiluminescence intensity can be used to determine the total heat release rate for the system.

References:

- [1] I. R. Hurley, R. B. Price, T. M. Sugden, A. Thomas, *Proc. of Roy. Soc. Lond. A.* 303 (1968) 409-427.
- [2] J. G. Lee, K. Kim, D. A. Santavicca, *Proc. Combust. Inst.* 28 (2000) 415- 421.
- [3] S. Kato, T. Fujimori, A. P. Dowling, H. Kobayashi, *Proc. Combust Inst.* 30 (2) (2005) 1799 -1806.
- [4] N. Swaminathan, G. Xu, A. P. Dowling, R. Balachandran, *J. Fluid Mech.* 681 (2011) 80-115.
- [5] S. Hemchandra, N. Peters, T. Liewwen, *Proc. Combust. Inst.* 33(1) (2011) 1609-1617.
- [6] Y. Liu, A. P. Dowling, N. Swaminathan, T. D. Dunstan, *Combust. Flame* 159(7) (2012) 2430-2440.
- [7] A. Gazi, G. Vourliotakis, G. Skevis, M. A. Founti, *Combust. Sci. Technol.* 2013, doi: 10.1080/00102202.2013.804517.
- [8] A. G. Gaydon, *The spectroscopy of flames*, 2nd Edition, Chapman and Hall Ltd., London, 1974.
- [9] J. -M. Samaniego, F. N. Egolfopoulos, C. T. Bowman, *Combust. Sci. Technol.* 109 (1995) 183-203.
- [10] J. -M. Samaniego, T. Mantel, *Combust. Flame* 118(4) (1999) 537-556.
- [11] Y. Hardalupas, M. Orain, *Combust. Flame* 139(3) (2004) 188-207.
- [12] T. Kathrotia¹, U. Riedel, J. Warnatz, A numerical study on the relation of OH*, CH* and C₂* chemiluminescence and heat release in premixed methane flames, 4th Proc. European Combustion meeting, 2009, Vienna University of Technology, Vienna, Austria.
- [13] Y. Hardalupas, C. S. Panoutsos, A. M. K. P. Taylor, *Exp Fluids* 49 (2010) 883-909.
- [14] L. C. Haber, U. Vandsburger, W. R. Saunders, V. K. Khanna, *Proc. Int. gas turbine Inst.* 2000-GT-021.
- [15] V. N. Nori, J. M. Seitzman, *Proc. Combust. Inst.* 32(1) (2009) 895-903.
- [16] M. Lauer, Sattelmayer T., *J. Eng. Gas Turb. Power* 132(1) (2010) 061502-1-8.
- [17] S. A. Farhat, W. B. Ng, Y. Zhang, *Fuel* 84 (2005) 1760-1767.
- [18] B. O. Ayoola, R. Balachandran, J. H. Frank, E. Mastorakos, C. F. Kaminski, *Combust. Flame* 144(1-2) (2006) 1-16.

- [19] M. Lauer, M. Zellhuber, T. Sattelmayer, C. J. Aul, *J. Eng. Gas Turb. Power* 133 (2011) 121501-8.
- [20] M. Röder, T. Dreier, C. Schulz, *Proc. Combust. Inst.* 34 (2013) 3349-3556.
- [21] M. Röder, T. Dreier, C. Schulz, *Appl. Phys. B* 107 (2012) 611- 617.
- [22] C. S. Panoutsos, Y. Hardalupas, A. M. K. P. Taylor, *Combust. Flame*, 156(2) (2009) 273-291.
- [23] H. N. Najm, P. H. Paul, C. J. Mueller, P. S. Wyckoff, *Combust. Flame* 113(3) (1998) 312-332.
- [24] J. Ballester, T. G. Armingol, *Prog. Eng. Combust. Sci.* 36(4) (2010) 375- 411.
- [25] M. D. Leo, A. Saveliev, L. A. Kennedy, S. A. Zelepouga, *Combust. Flame* 149(4) (2007) 435-445.
- [26] Y. Nakamura, Y. Yamashita, K. Saito, *Combust. Theor. Model.* 10(6) (2006) 927-938.
- [27] R. Mattsson, M. Kupianinen, P. Gren, A. Wåhlin, T. E. Carlsson, C. Fureby, *Combust. Flame* 139(1-2) (2004) 1-15.
- [28] J. O. Hirschfelder, M. A. Eliason, *Ann. NY. Acad. Sci.* 67 (1957) 451-461.
- [29] J. Kojima, Y. Ikeda, T. Nakajima, *Combust. Flame* 140(1-2) (2005) 34- 45.
- [30] J. M. Hall, D. J. Varies, A. R. Amadio, E. L. Petersen, Towards a kinetics Model of CH chemiluminescence, 43rd AIAA Aerospace Sciences Meeting and Exhibit, 2005, Reno, Nevada, USA.
- [31] CHEMKIN-Pro release 15101, March 27, 2013, available at>
< <http://www.reactiondesign.com/products/open/chemkin-pro.html>>
- [32] G. P. Smith et al., GRI-Mech 3.0, March 27, 2013, available at:
<<http://www.me.berkeley.edu/gri-mech/version30/text30.html>>
- [33] Hai-Wang's mechanism (HW-Mech), March 27, 2013, available at:
<<http://ignis.usc.edu/Mechanisms/C3-opt/C3-opt.html>>
- [34] San Diego Mechanism (SD-Mech), March 27, 2013, available at:
<<http://web.eng.ucsd.edu/mae/groups/combustion/mechanism.html>>
- [35] N. V. Nori, M. J. Seitzman, Evaluation of chemiluminescence as combustion diagnostic under varying operating conditions, 46th AIAA Aerospace Sciences Meeting and Exhibit, 2008, Reno, Nevada, USA.

- [36] N. V. Nori, M. J. Seitzman, Chemiluminescence measurements and modelling in syngas, Methane and Jet-A fuelled combustors, 45th AIAA Aerospace Sciences Meeting and Exhibit, 2007, Reno, Nevada, USA.
- [37] K. T. Walsh, M. B. Long, M. A. Tanoff, M. D. Smooke, *Proc. Combust. Inst.* 27 (1998) 615–623.
- [38] Burcat's Thermodynamic Data, March 27, 2013, available at:
< <http://garfield.chem.elte.hu/Burcat/burcat.html> >
- [39] M. Tamura, P. A. Berg, J. E. Harrington, J. Luque, J.B. Jeffries, G. P. Smith, D. R. Crosley, *Combust. Flame* 114(3-4) (1998) 502-514.
- [40] H. Böhm, K. Hohse-Höinghaus, F. Lacas, C. Rolon, N. Darabiha, S. Candel, *Combust. Flame* 124(1-2) (2001) 127-136.
- [41] H. Wang, M. Frenklach, *Combust. Flame* 110 (1997) 173-221.
- [42] M. Mével, S. Javoy, K. Coudoro, G. Durpé, C.-E. Pillard, *Int. J. Hydrogen Energy* 37 (2012) 689-714.
- [43] B. Prabasena, M. Röder, T. Kathrotia, U. Riedel, T. Dreier, C. Schulz, *Appl. Phy. B* 107 (2012) 561- 569.

List of captions of tables

Table 1 Sub-reaction mechanism to model the production/consumption of OH* and CH* [35]

Table 2 Lennard-Jones collision diameter (σ) & Lennard-Jones potential well depth (ϵ)

Table 3 Comparison of the peak values of the mole fraction of CH* with and without PAH (polycyclic aromatic hydrocarbon) formation kinetics

List of captions of figures

Fig. 1 Typical flame structure including the spatial profile of heat release rate (HRR) and concentration of CH* ($[CH^*]$) for (a) methane-air and (b) propane-air flames when different sub-reaction models for excited radicals are applied using GRI-Mech 3.0 [32] for the ground state species (ejection velocity: 0.5 m/s).

Fig. 2 The major reactions for the production/consumption rate of CH* (a) for methane-air and (b) for propane-air flames when different sub-reaction models for excited radicals are applied with GRI-Mech 3.0 [32] for ground state species.

Fig. 3 The influence of detail reaction mechanisms on the production/consumption rate of CH* for a methane-air flame over a wide range of velocity conditions (Nori's model was applied for the excited radicals).

Fig. 4a Correlation between the local heat release rate (HRR) and local concentration of CH* ($[CH^*]$) for a non-dilute methane-air flame.

Fig. 4b Characteristics of the spatial heat release rate (HRR) and spatial concentration of CH* ($[CH^*]$) profiles for a non-dilute methane-air flame with different velocities

Fig. 5 Influence of fuel types on the correlation between total chemiluminescence from CH* and the total heat release rate under various velocity conditions.

Fig. 6 Influence of a detail reaction mechanism on the correlation between total chemiluminescence from CH* and the total heat release rate under various velocity conditions (Nori's sub-reaction model for excited radicals was applied).

Fig. 7 Influence of sub-reaction models on the correlation between total chemiluminescence from CH* and the total heat release rate under various velocity conditions for a methane-air flame (GRI-Mech 3.0 is applied as the detail reaction mechanism for the ground state species).

Fig. 8 Influence of diluents on the correlation between total chemiluminescence from CH* and the total heat release rate under various velocity conditions for a methane-air flame.

Fig. 9 Influence of the excited radical transport properties on the correlation between the total chemiluminescence from CH* and total heat release rate for methane-air flames under various velocity conditions.

Fig.10 Observation of the reaction path when CH* is produced from (a) methane-air flame and (b) propane-air flame at a velocity of 0.5 m/s.

Fig. 11 C₂H production prediction by three different detail reaction mechanisms (GRI-Mech 3.0 [32], HW-Mech [33], and SD-Mech [34]) for a methane-air flame with an applied velocity of 0.5 m/s (Nori's sub reaction model for excited radicals is applied).

Fig. 12 The distribution of the maximum temperature (T_{max}), total chemiluminescence (TCL), and total heat release rate (THRR) with and without dilution for methane-air flames at various applied velocities.

Fig. 13 Reaction sensitivities for the production/consumption (mole/cm³·s) of C₂H in a methane-air flame at a velocity of 0.5 m/s (no diluent).

Fig. 14 The distribution of the peak values of the production/consumption of C_2H and the mole fraction of CH^* against a wide range of applied velocities for a methane-air flame (no diluents).

Fig. 15 Mole fraction profiles of CH^* over the distance from the fuel port against a wide range of applied velocities for methane-air flames.

Fig. 16 The mole fraction profiles for C_2H_2 over distances from the fuel port against a wide range of applied velocity for methane-air flames.

Fig.17 The distribution of mole fraction profiles of C_2H_2 , C_2H , OH , and CH^* for methane-air flames (applied velocity: 3.0 m/s).

Fig.18 Comparison of the peak values of the mole fraction of CH^* in the present study with values from the study of Prabasena, et al. [43] over an applied velocity range of 1.0 m/s to 3.5 m/s.

Table 1 Sub-reaction mechanism to model the production/consumption of OH* and CH* [35]

No.	Reaction	A (cm ³ /(mole · s))	b	E (cal/mol)
1.	H + O + M ↔ OH* + M	6.00×10 ¹⁴	0.0	6940
2.	CH + O ₂ ↔ OH* + CO	3.24×10 ¹⁴	-0.4	4150
3.	OH* + H ₂ O → OH + H ₂ O	5.92 ×10 ¹²	0.5	-861
4.	OH* + CO ₂ → OH + CO ₂	2.75×10 ¹²	0.5	-968
5.	OH* + CO → OH + CO	3.23×10 ¹²	0.5	-787
6.	OH* + H ₂ → OH + H ₂	2.95×10 ¹²	0.5	-444
7.	OH* + O ₂ → OH + O ₂	2.10×10 ¹²	0.5	-482
8.	OH* + OH → OH + OH	1.50×10 ¹²	0.5	0.0
9.	OH* + H → OH + H	1.50×10 ¹²	0.5	0.0
10.	OH* + O → OH + O	1.50×10 ¹²	0.5	0.0
11.	OH* + N ₂ → OH + N ₂	1.08×10 ¹¹	0.5	-1238
12.	OH* + CH ₄ ↔ OH + CH ₄	3.36×10 ¹²	0.5	-635
13.	C ₂ H + O ↔ CH* + CO	6.023×10 ¹²	0.0	457
14.	C ₂ H + O ₂ ↔ CH* + CO ₂	6.023×10 ⁻⁴	4.4	-2285.1
15.	CH* + H ₂ O ↔ CH + H ₂ O	5.30×10 ¹³	0.0	0.0
16.	CH* + CO ₂ ↔ CH + CO ₂	2.41×10 ⁻¹	4.3	-1694
17.	CH* + CO ↔ CH + CO	2.44×10 ¹²	0.5	0.0
18.	CH* + H ₂ ↔ CH + H ₂	1.47×10 ¹⁴	0.0	1361
19.	CH* + O ₂ ↔ CH + O ₂	2.48×10 ⁶	2.14	-1720
20.	CH* + N ₂ ↔ CH + N ₂	3.03×10 ²	3.4	-381
21.	CH* + CH ₄ → CH + CH ₄	1.73×10 ¹³	0.0	167

Note : The reaction rate coefficient is expressed as $k = AT^b \exp(-E/RT)$,

where A is a pre-exponential factor; T is the temperature; b is the temperature exponent; E is the activation energy; and R is the universal gas constant.

Table 2 Lennard-Jones collision diameter (σ) & Lennard-Jones potential well depth (ϵ)

Case	Description	
Case I	$\sigma_{OH^*} = \sigma_{OH}$; $\epsilon_{OH^*} = \epsilon_{OH}$ $\sigma_{CH^*} = \sigma_{CH}$; $\epsilon_{CH^*} = \epsilon_{CH}$	
Case II	$\epsilon_{OH^*} = \epsilon_{OH}$ and $\epsilon_{CH^*} = \epsilon_{CH}$	$\sigma_{OH^*} = 0.25 \times \sigma_{OH}$; $\sigma_{CH^*} = 0.25 \times \sigma_{CH}$
Case III		$\sigma_{OH^*} = 4.0 \times \sigma_{OH}$; $\sigma_{CH^*} = 4.0 \times \sigma_{CH}$
Case IV	$\sigma_{OH^*} = \sigma_{OH}$ and $\sigma_{CH^*} = \sigma_{CH}$	$\epsilon_{OH^*} = 0.25 \times \epsilon_{OH}$; $\epsilon_{CH^*} = 0.25 \times \epsilon_{CH}$
Case V		$\epsilon_{OH^*} = 4.0 \times \epsilon_{OH}$; $\epsilon_{CH^*} = 4.0 \times \epsilon_{CH}$

Table 3 Comparison of the peak values of the mole fraction of CH* with and without PAH (polycyclic aromatic hydrocarbon) formation kinetics

Applied velocity (m/s)	Mole fraction of CH* [-] (100% CH ₄ + 0% N ₂)	
	With polycyclic aromatic hydrocarbon (PAH) formation kinetics [41]	Without polycyclic aromatic hydrocarbon (PAH) formation kinetics
0.1	2.64 x 10 ⁻¹¹	2.67 x 10 ⁻¹¹
0.5	1.18 x 10 ⁻¹⁰	1.24 x 10 ⁻¹⁰
1.0	1.90 x 10 ⁻¹⁰	2.01 x 10 ⁻¹⁰
1.5	2.27 x 10 ⁻¹⁰	2.41 x 10 ⁻¹⁰
2.0	2.44 x 10 ⁻¹⁰	2.48 x 10 ⁻¹⁰
2.5	2.31 x 10 ⁻¹⁰	2.38 x 10 ⁻¹⁰

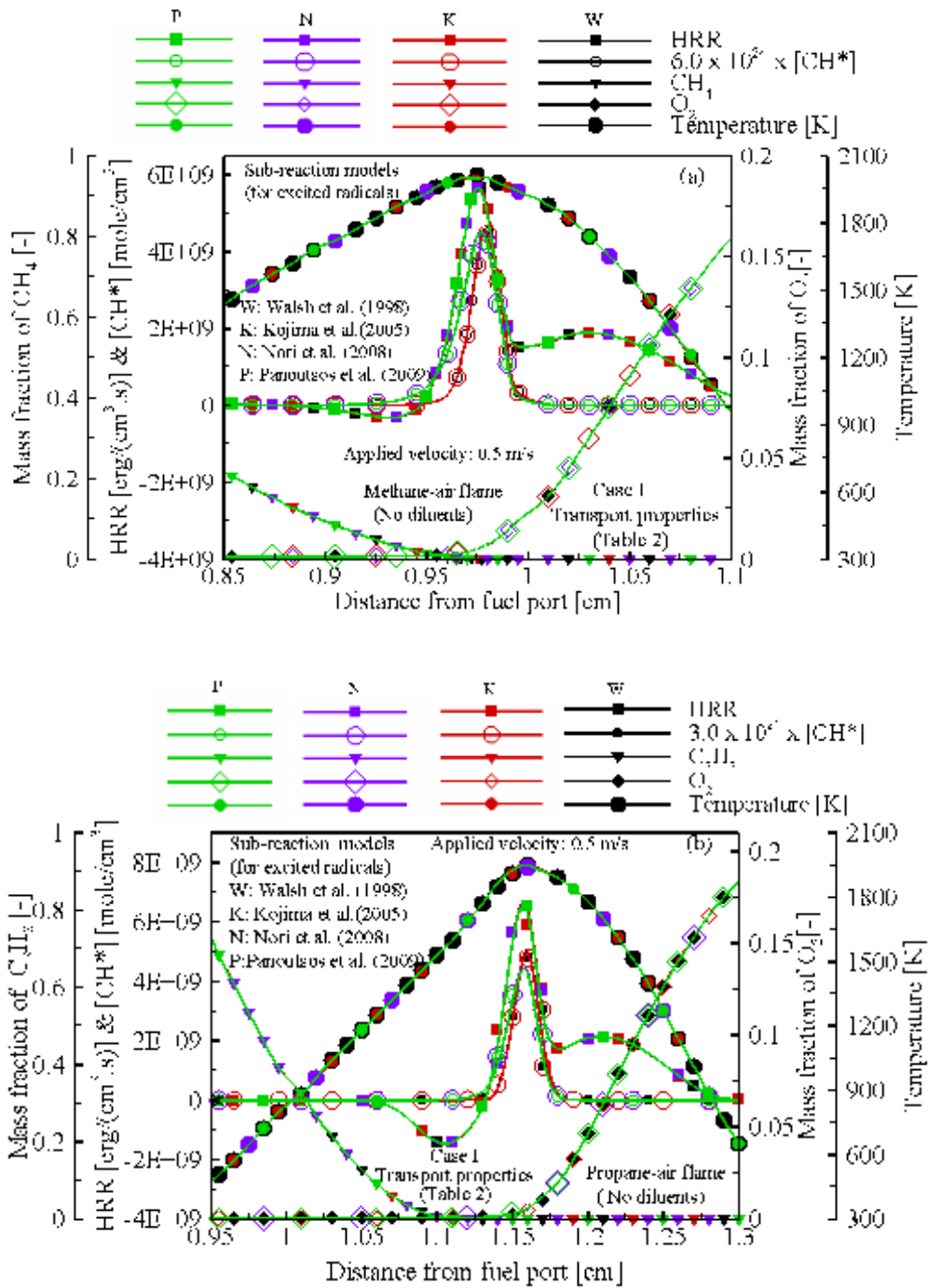


Fig. 1 Typical flame structure including the spatial profile of heat release rate (HRR) and concentration of CH^* ($[\text{CH}^*]$) for (a) methane-air and (b) propane-air flames when different sub-reaction models for excited radicals are applied using GRI-Mech 3.0 [32] for the ground state species (ejection velocity: 0.5 m/s).

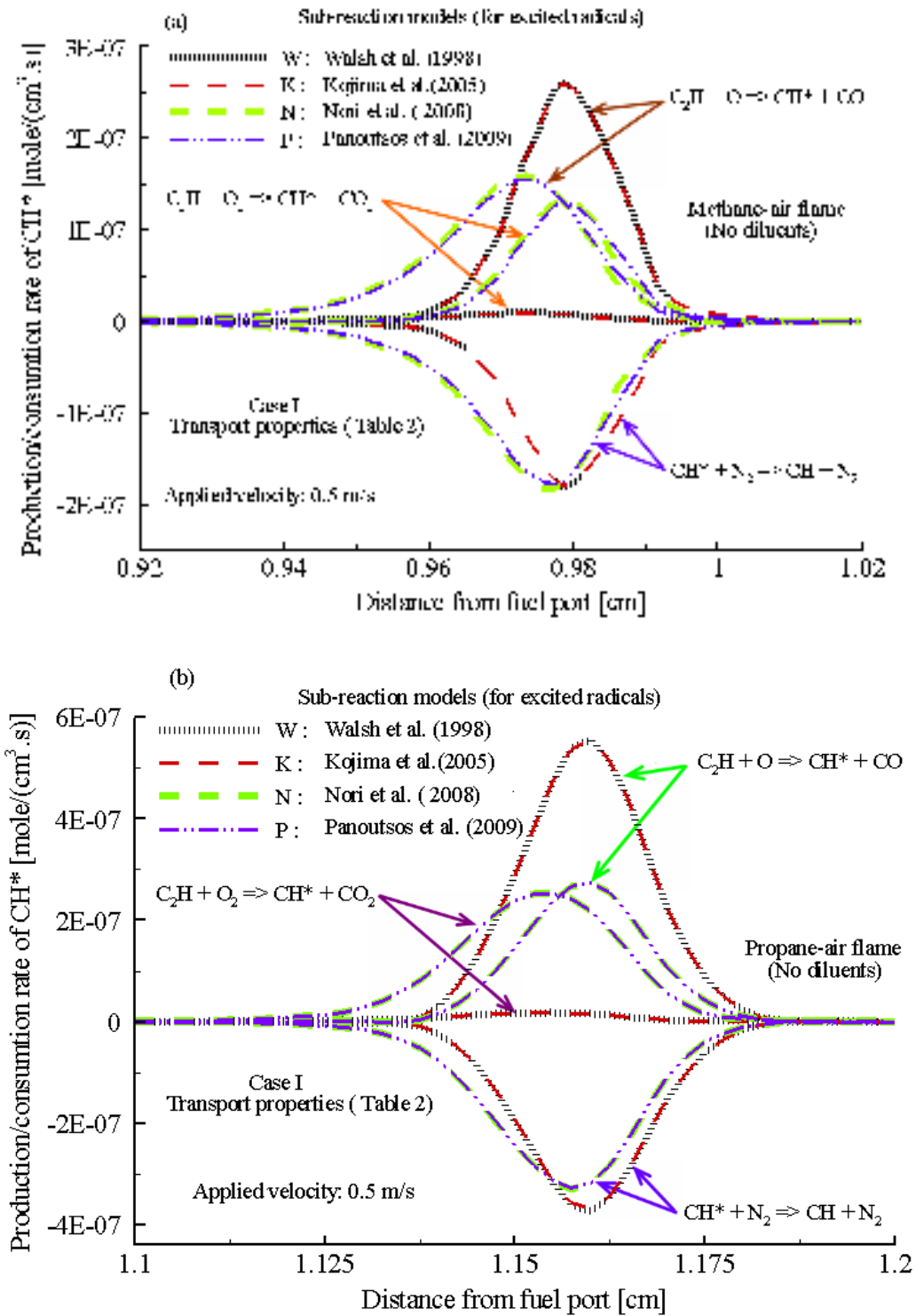


Fig. 2 The major reactions for the production/consumption rate of CH^* (a) for methane-air and (b) for propane-air flames when different sub-reaction models for excited radicals are applied with GRI-Mech 3.0 [32] for ground state species.

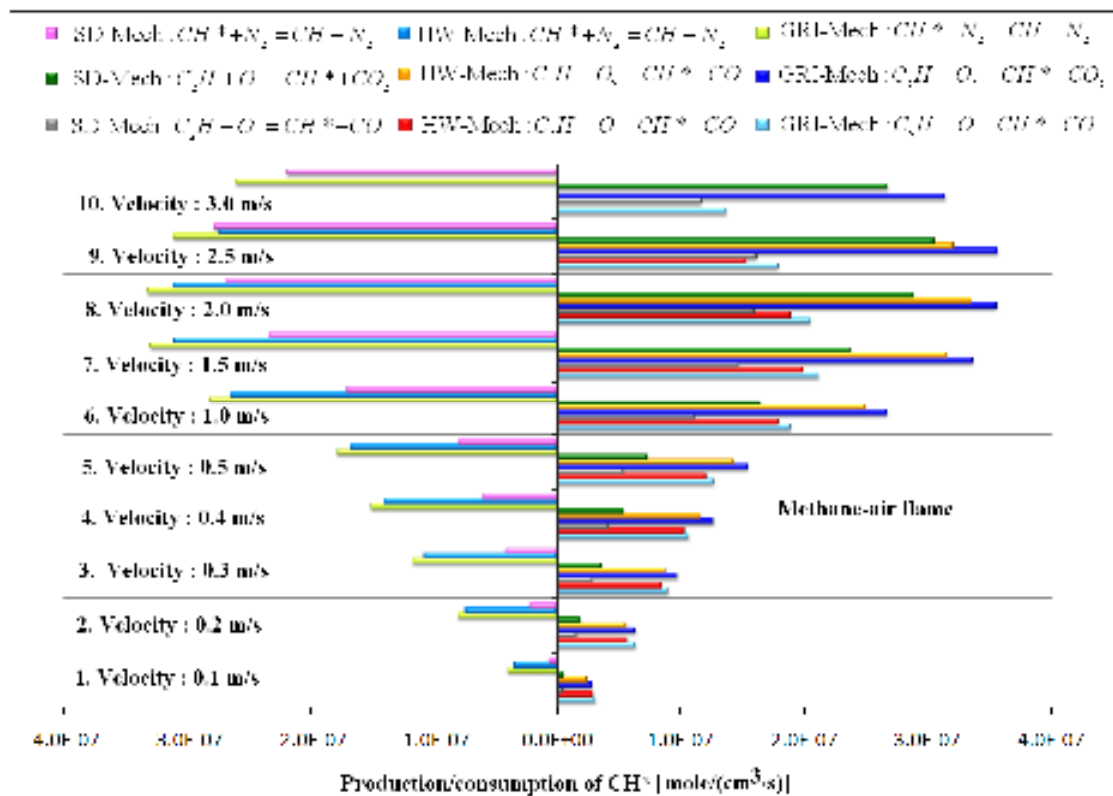


Fig. 3 The influence of detail reaction mechanisms on the production/consumption rate of CH^* for a methane-air flame over a wide range of velocity conditions (Nori's model was applied for the excited radicals).

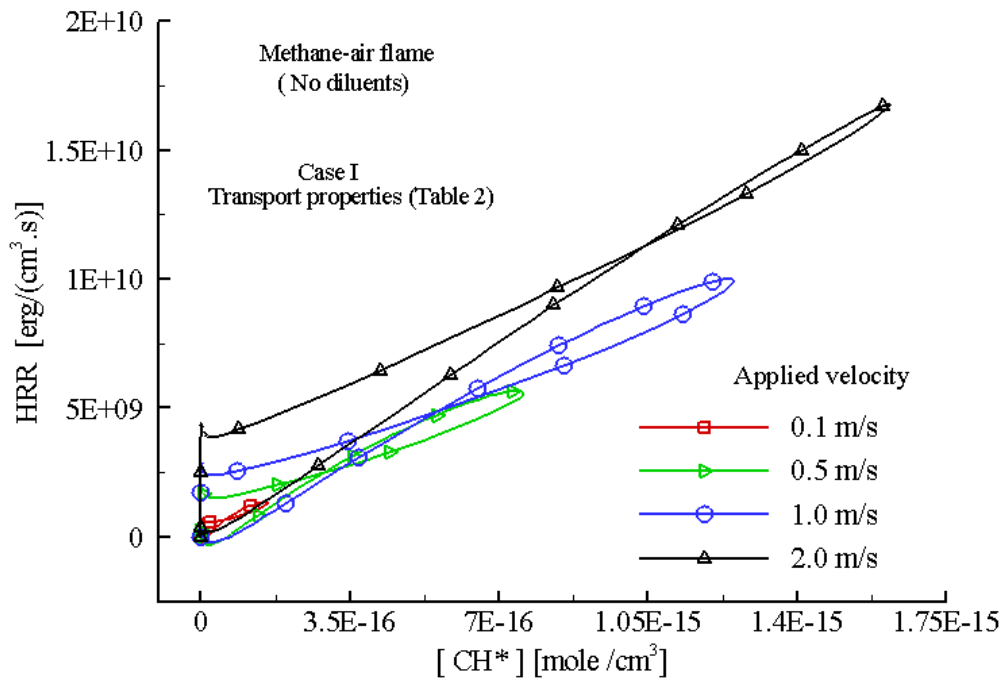


Fig. 4a Correlation between the local heat release rate (HRR) and local concentration of CH* ([CH*]) for a non-dilute methane-air flame.

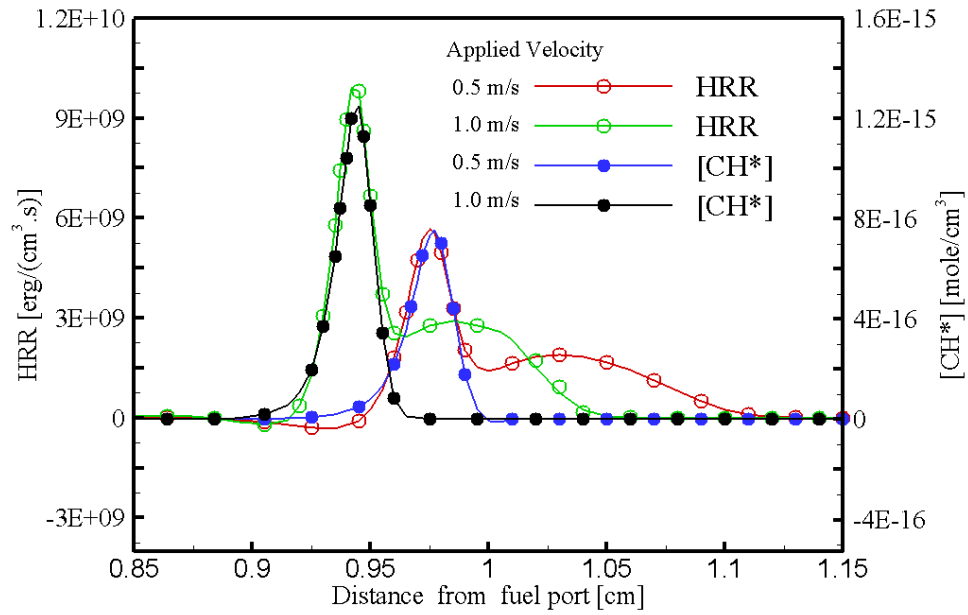


Fig. 4b Characteristics of the spatial heat release rate (HRR) and spatial concentration of CH* ([CH*]) profiles for a non-dilute methane-air flame with different velocities

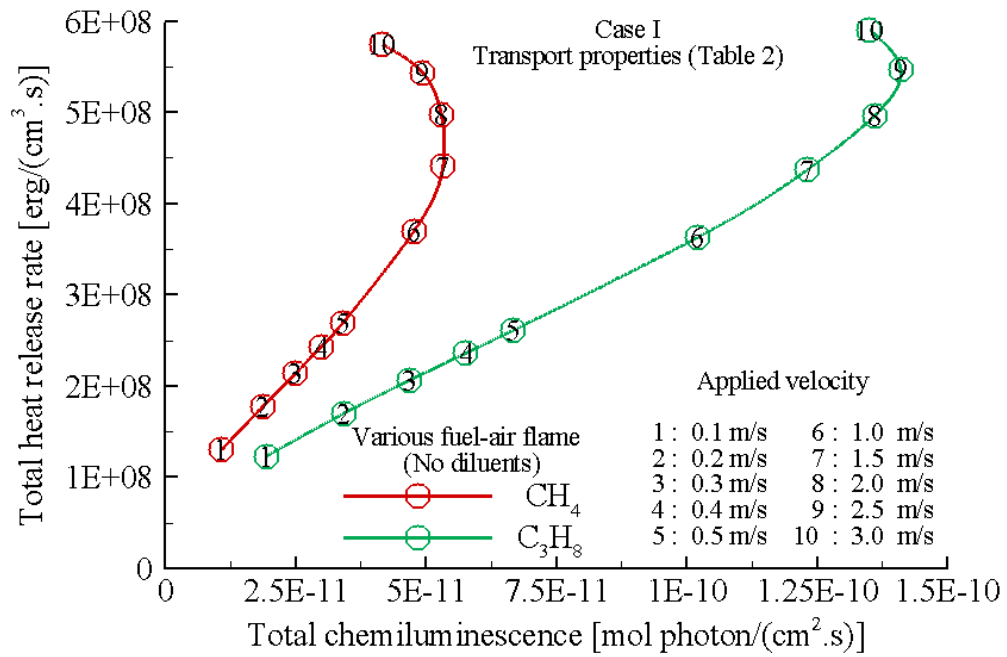


Fig. 5 Influence of fuel types on the correlation between total chemiluminescence from CH* and the total heat release rate under various velocity conditions.

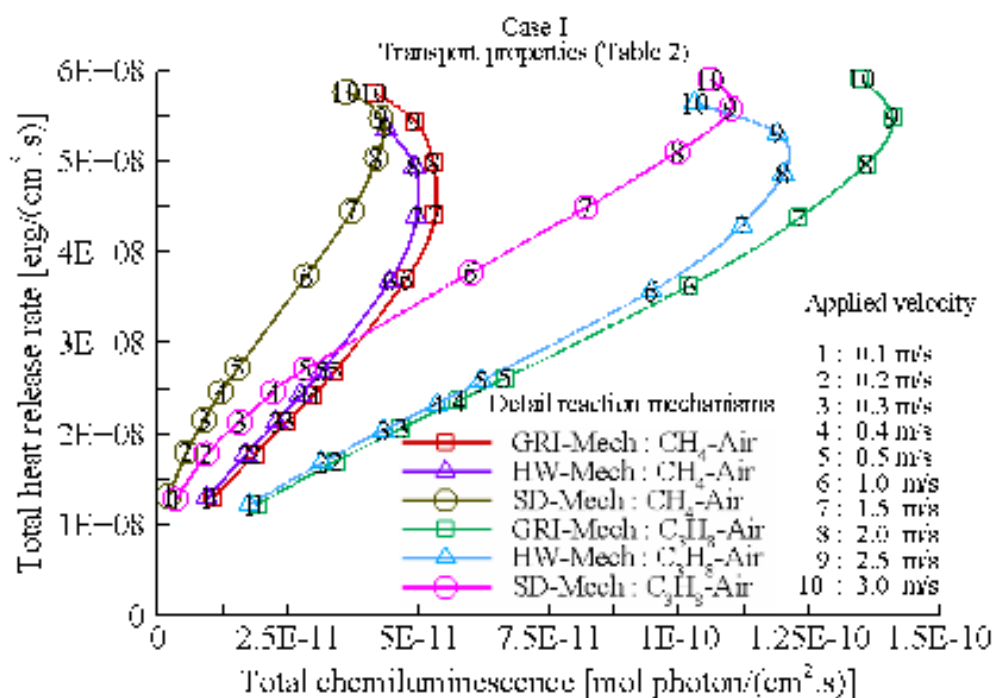


Fig. 6 Influence of a detail reaction mechanism on the correlation between total chemiluminescence from CH* and the total heat release rate under various velocity conditions (Nori's sub-reaction model for excited radicals was applied).

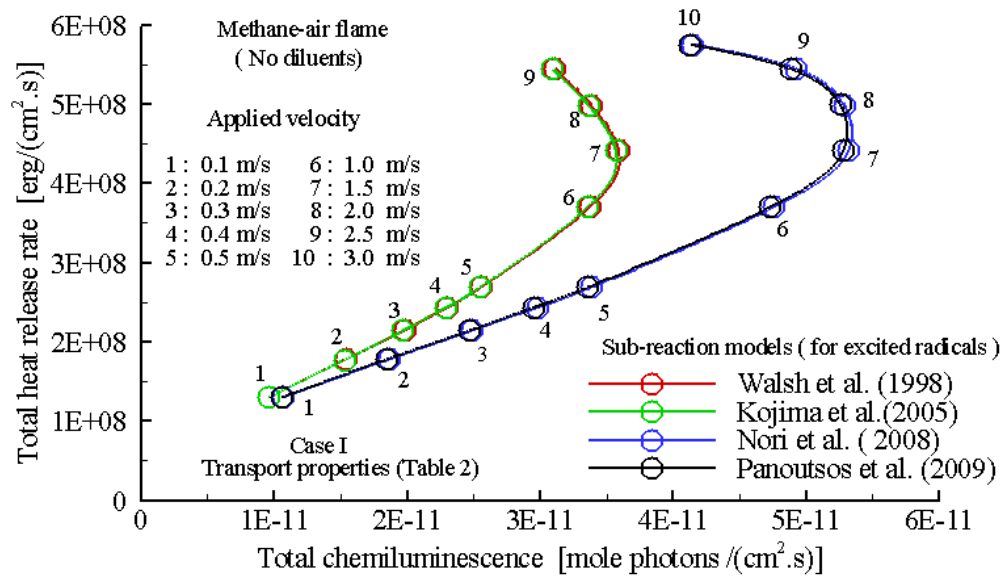


Fig. 7 Influence of sub-reaction models on the correlation between total chemiluminescence from CH^* and the total heat release rate under various velocity conditions for a methane-air flame (GRI-Mech 3.0 is applied as the detail reaction mechanism for the ground state species).

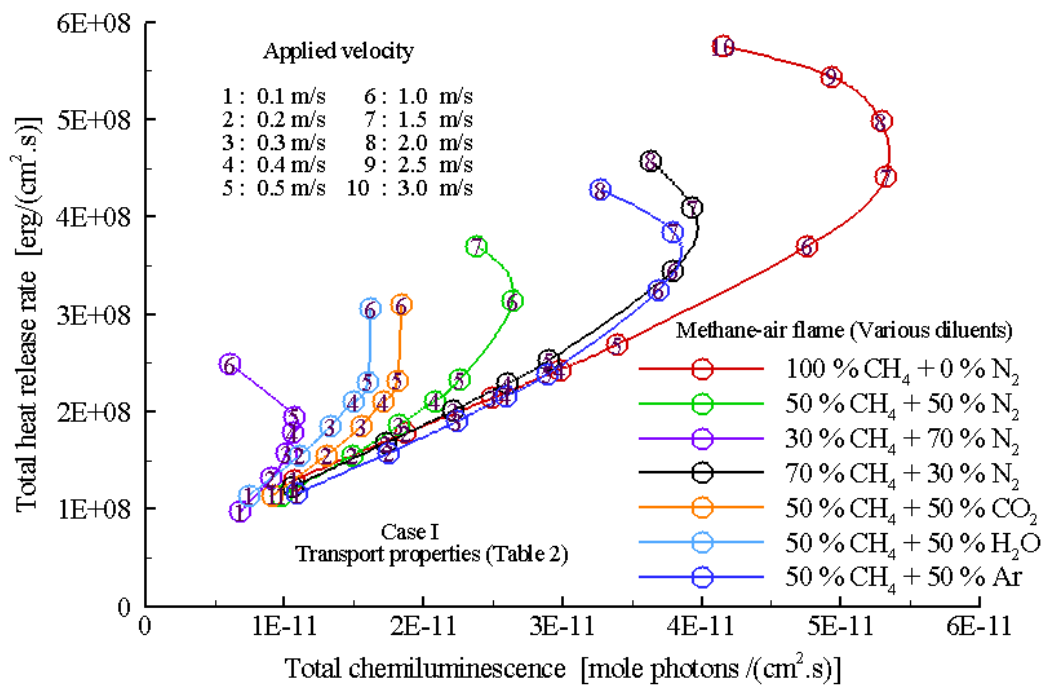


Fig. 8 Influence of diluents on the correlation between total chemiluminescence from CH* and the total heat release rate under various velocity conditions for a methane-air flame.

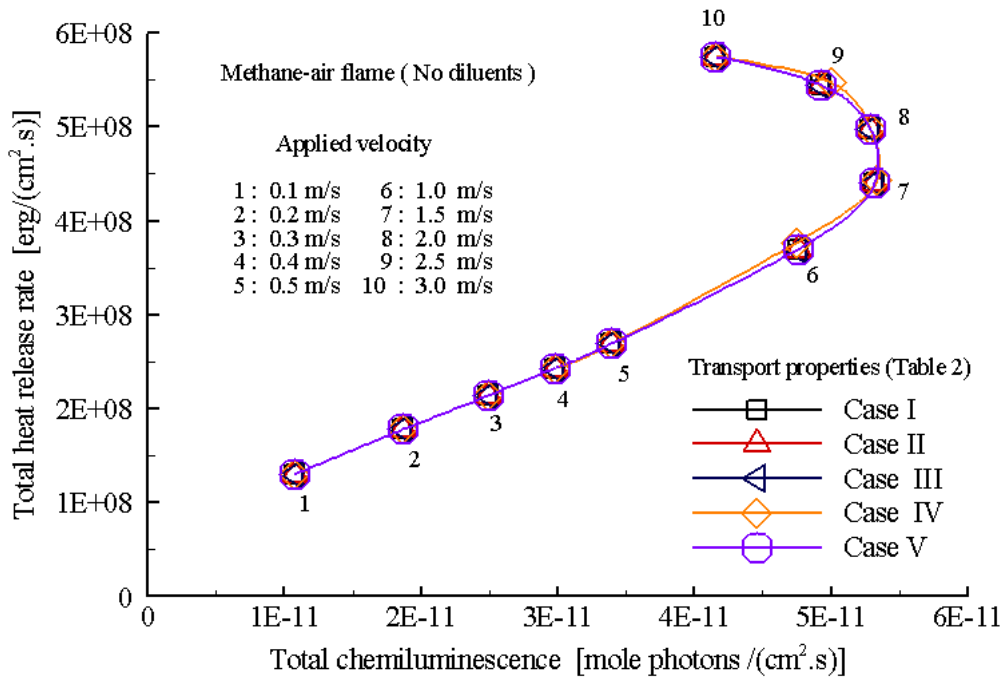


Fig. 9 Influence of the excited radical transport properties on the correlation between the total chemiluminescence from CH* and total heat release rate for methane-air flames under various velocity conditions.

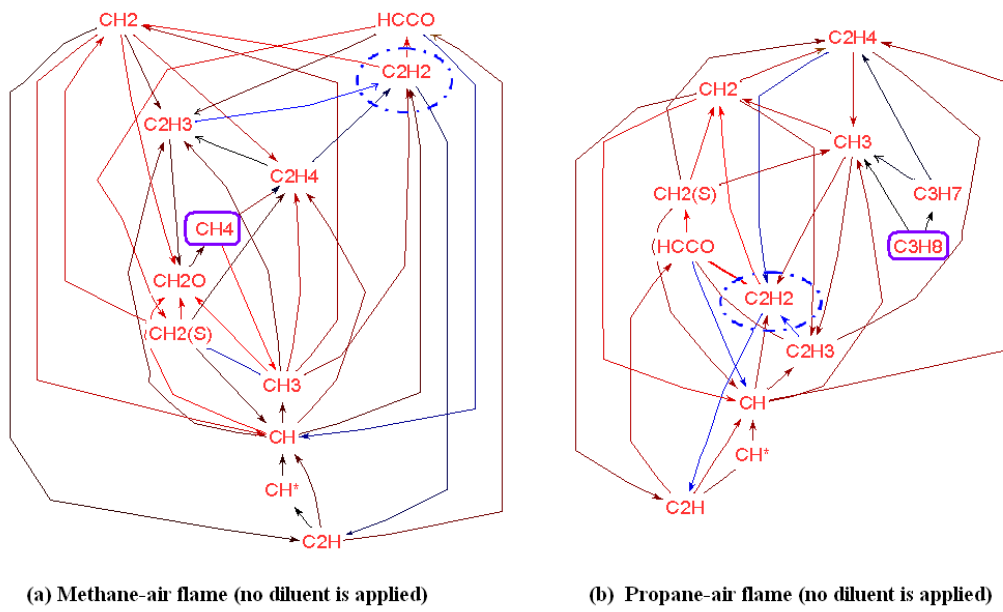


Fig.10 Observation of the reaction path when CH^* is produced from (a) methane-air flame and (b) propane-air flame at a velocity of 0.5 m/s.

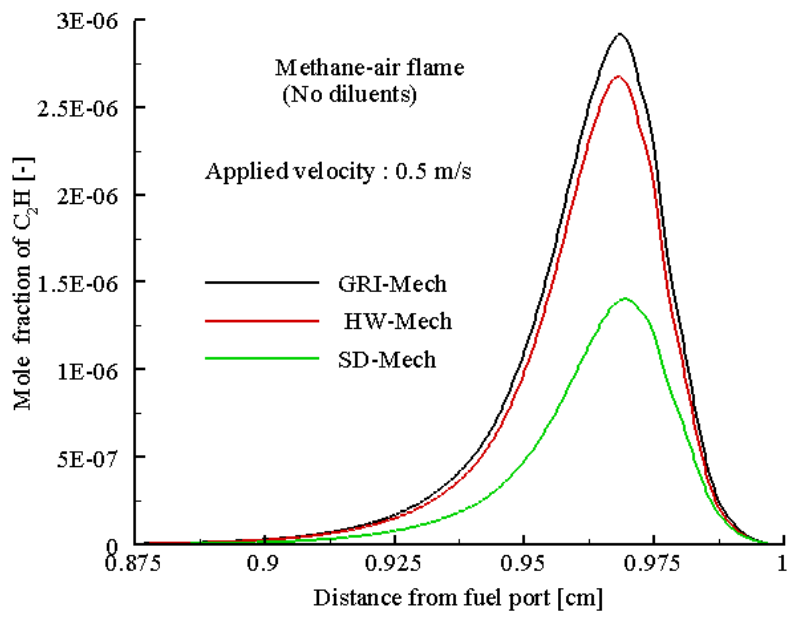


Fig. 11 C_2H production prediction by three different detail reaction mechanisms (GRI-Mech 3.0 [32], HW-Mech [33], and SD-Mech [34]) for a methane-air flame with an applied velocity of 0.5 m/s (Nori's sub reaction model for excited radicals is applied).

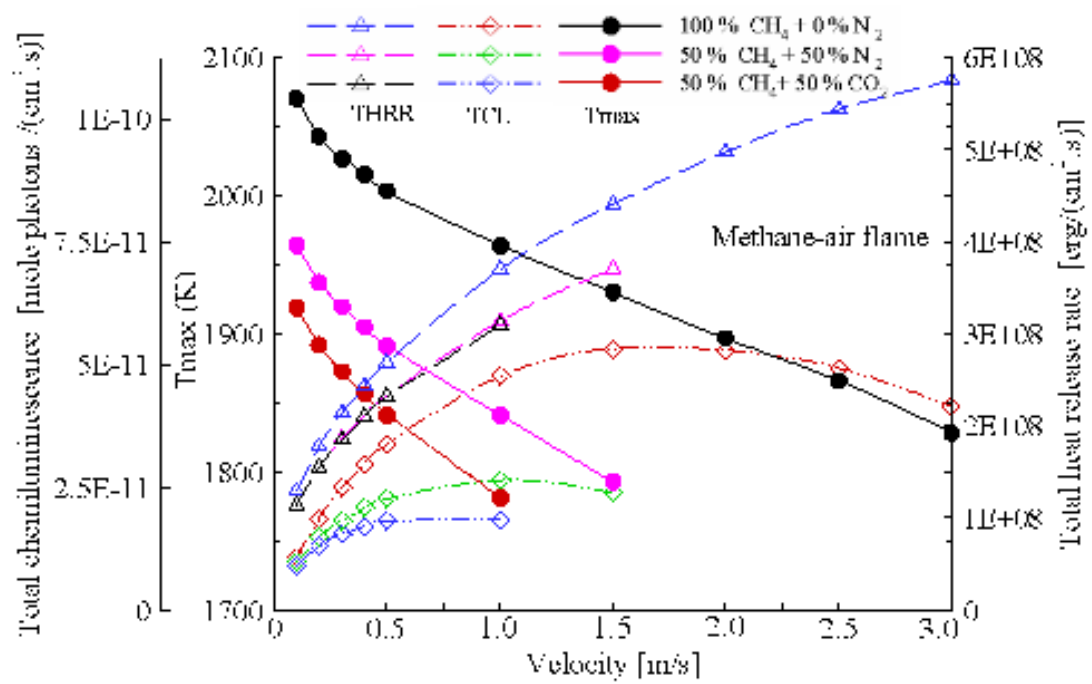


Fig. 12 The distribution of the maximum temperature (T_{max}), total chemiluminescence (TCL), and total heat release rate (THRR) with and without dilution for methane-air flames at various applied velocities.

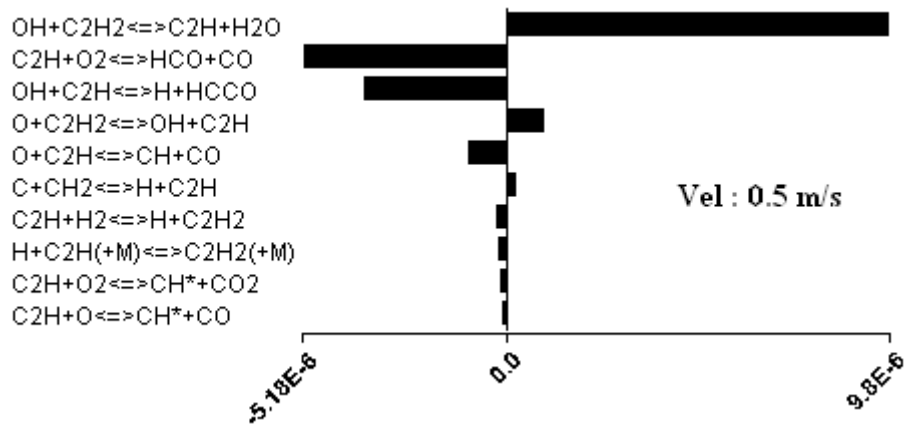


Fig. 13 Reaction sensitivities for the production/consumption (mole/cm³·s) of C₂H in a methane-air flame at a velocity of 0.5 m/s (no diluent).

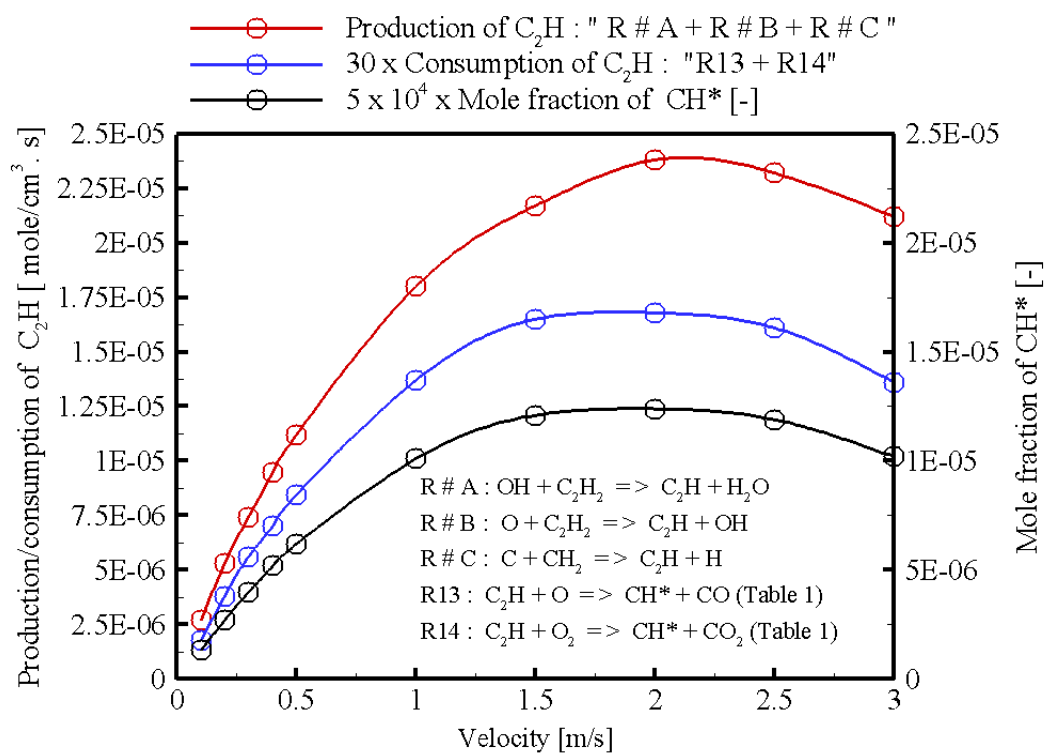


Fig. 14 The distribution of the peak values of the production/consumption of C_2H and the mole fraction of CH^* against a wide range of applied velocities for a methane-air flame (no diluents).

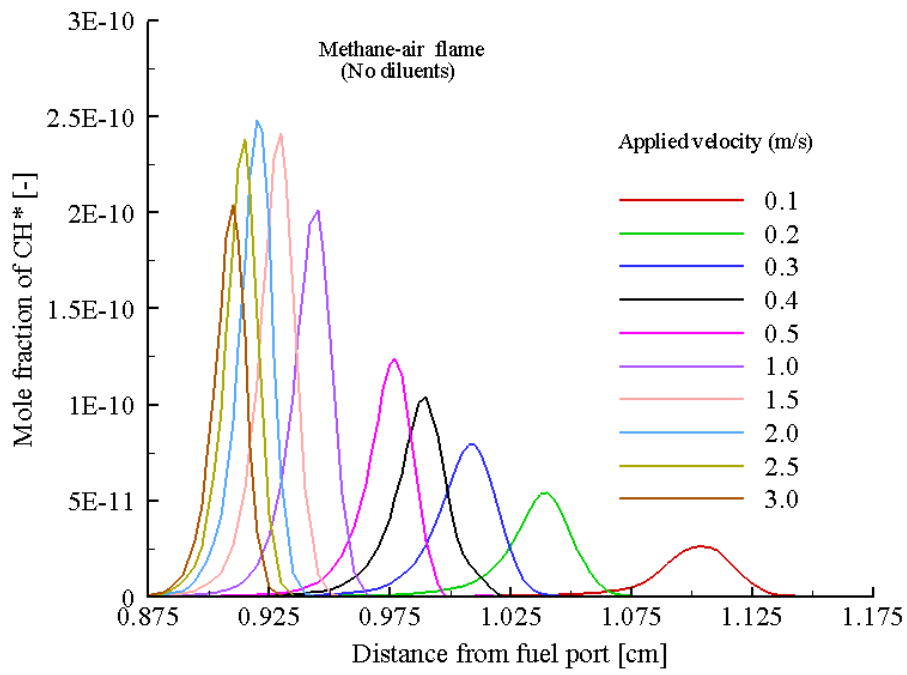


Fig. 15 Mole fraction profiles of CH* over the distance from the fuel port against a wide range of applied velocities for methane-air flames.

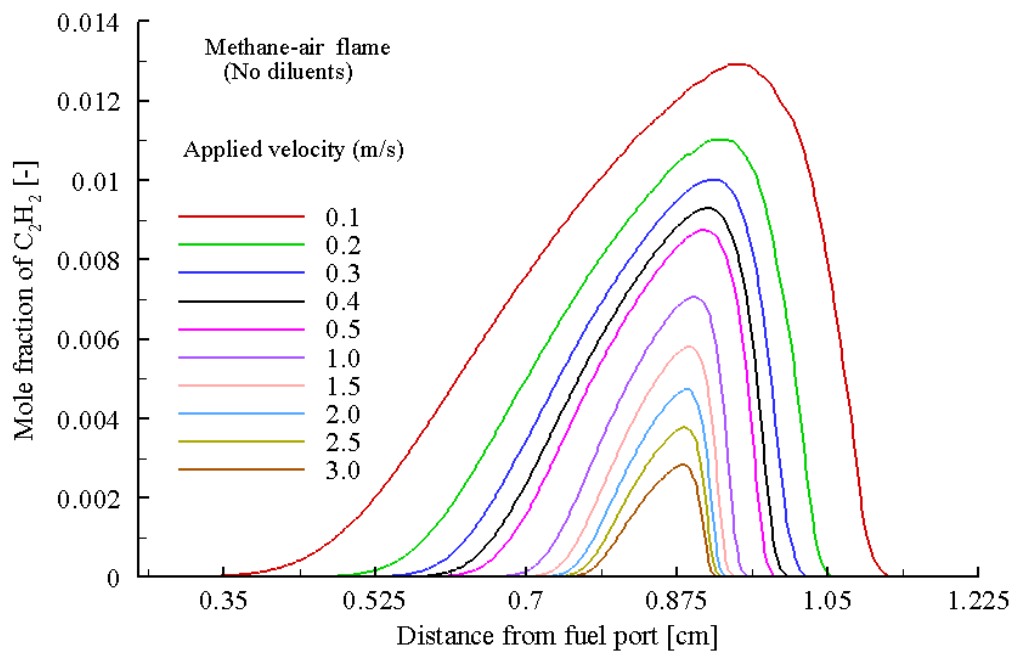


Fig. 16 The mole fraction profiles for C₂H₂ over distances from the fuel port against a wide range of applied velocity for methane-air flames.

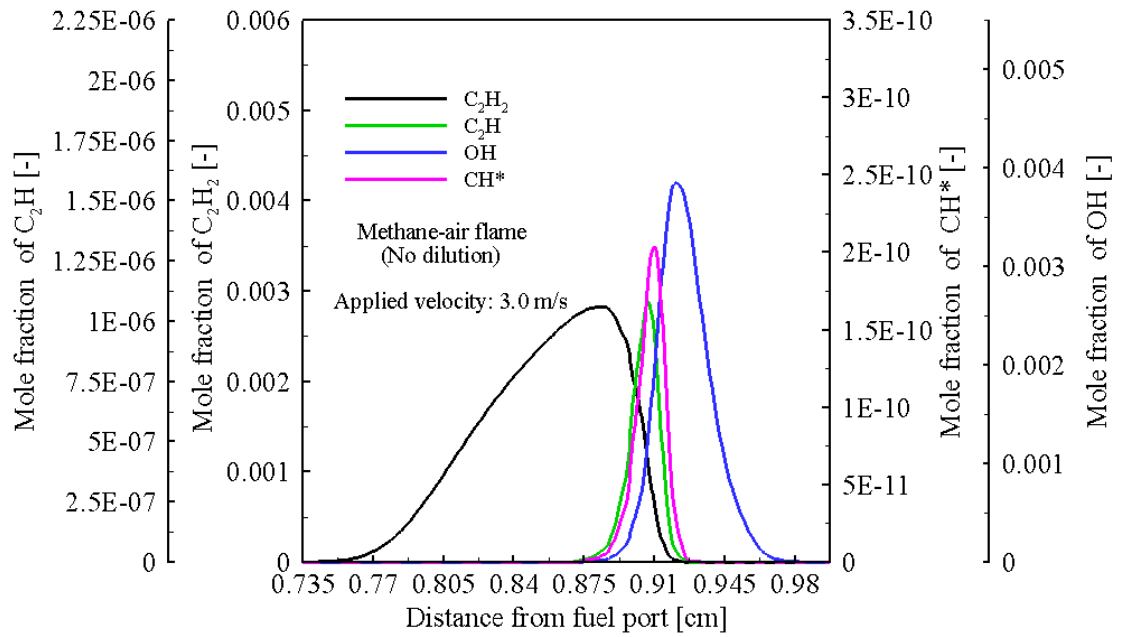


Fig.17 The distribution of mole fraction profiles of C_2H_2 , C_2H , OH , and CH^* for methane-air flames (applied velocity: 3.0 m/s).

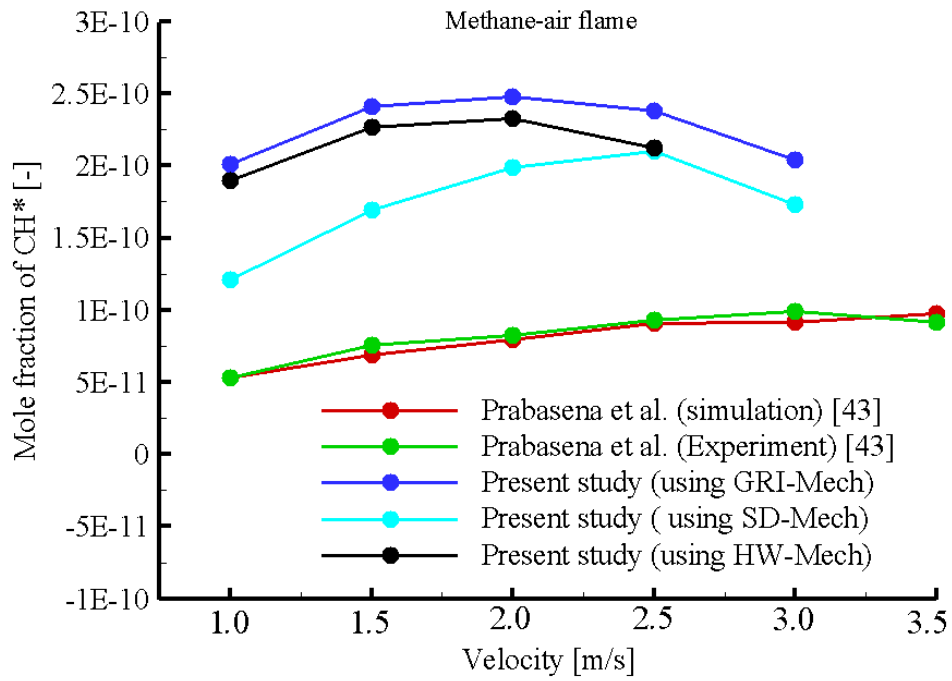


Fig.18 Comparison of the peak values of the mole fraction of CH* in the present study with values from the study of Prabasena, et al. [43] over an applied velocity range of 1.0 m/s to 3.5 m/s.